Supporting Information

Villinger et al. 10.1073/pnas.1012310108

SI Text

SI Materials and Methods. ***Preparation of human VDAC1.*** Expression, refolding, and purification of wild type (WT) and E73V hVDAC1 was done mostly as described in ref. 1. According to previous findings (2), a His6-Tag was attached to the C terminus of hVDAC1 to improve the overall folding properties of the protein. Improved sample purification (3) was applied to hVDAC1 preparations. Functionality of our hVDAC1 preparation was confirmed by electrophysiological measurements in lipid bilayers as described in 1.

NMR spectroscopy. NMR spectra were recorded on ^{2}H(75%)-^{15}N or ^{2}H(75%)-^{13}C-^{15}N labeled samples containing 0.5–0.8 mM hVDAC1, 25 mM BisTris pH 6.8, approximately 250 mM lauryl-dimethylamine-N-oxide (LDAO), and 5–10% D_2O. All spectra were measured at 37 °C (unless stated otherwise) on Bruker 800 or 900 MHz spectrometers equipped with cryogenic probes. Spectra were processed using NMRPipe (4) and analyzed with SPARKY (5).

To further improve the previously obtained backbone resonance assignment (2), TROSY-based HNCA experiments (6) were recorded on samples with improved purity, and two-dimensional ^{1}H,^{15}N-TROSY experiments (7) at varying temperatures (37 °C, 32 °C, 27 °C, and 22 °C) were used to discriminate overlapping peaks. In addition, N^H and C_α chemical shifts assigned by solid state NMR in the N-terminal helix (8) were taken into consideration.

Peak intensities for WT VDAC1 were collected in triplicate and averaged, using two ^{1}H,^{15}N-TROSY spectra and one reference spectrum of a heteronuclear NOE experiment applying no saturation. To exclude exchange of amide protons with saturated water protons, water flip-back pulse sequences were used (7). All ^{1}H,^{15}N-TROSY spectra were measured with $1{,}024 \times 256$ total points and 24–48 scans, and peak intensities were scaled according to the number of scans and the protein concentration.

Steady state heteronuclear {^{1}H},^{15}N-NOEs were measured employing the TROSY scheme (9). Heteronuclear NOE values are reported as the ratio of peak intensities in paired interleaved spectra collected with and without initial proton saturation period (4 s) during the 5-s-recycle delay. The two experiments were measured with $1{,}024 \times 202$ total points each and 120 scans.

Chemical exchange rates (R_{ex}) were determined from a set of three TROSY-based pulse sequences (10) used to obtain peak intensities $I^{\mathrm{N_xH_\alpha^N}}$, $I^{\mathrm{N_xH_\beta^N}}$, and $I^{\mathrm{2N_zH_z^N}}$. The three spectra were measured interleaved with $1{,}024 \times 244$ total points and 240 scans for WT hVDAC1 and $1{,}024 \times 148$ total points and 320 scans for E73V hVDAC1. The shortest possible relaxation delay of $2\tau = 1/J = 10.87$ ms was used, corresponding to $I^{\mathrm{N_xH_\beta^N}}/I^{\mathrm{N_xH_\alpha^N}}$ of 0.2 for most residues. R_{ex} was determined as (10):

$$R_{\mathrm{ex}} = R_2^{\mathrm{N_xH_\alpha^N}} - R_1^{\mathrm{2HzNz}}/2 - \eta_{xy}(\kappa - 1). \qquad \textbf{[S1]}$$

κ was estimated by the mean of $1 + (R_2^{\mathrm{N_xH_\alpha^N}} - R_1^{\mathrm{2HzNz}}/2)/\eta_{xy}$ using all residues in β-strands that were apparently not exchanging in WT hVDAC1 (β8–β11, β14–β15, and β18), resulting in a value of 1.15 (1.17) for WT (E73V) hVDAC1. For nonexchanging residues ($-10 < R_{\mathrm{ex}} < +10$), R_{ex} is distributed around 0.75 s^{-1} (0.65 s^{-1}) with a standard deviation of 5 s^{-1} due to variation in magnitude and orientation of the ^{15}N CSA tensor (11). Very weak peaks that resulted in unusually negative values for R_{ex} were excluded from the analysis (5/6 residues in total for WT/E73V hVDAC1).

For the reaction of hVDAC1 with DCCD (Calbiochem-Novabiochem), the chemical was added to WT hVDAC1 from a stock solution in dimethylformamide (DMF)-d7 to a final concentration of 2 mM (final 1% DMF-d7). ^{1}H,^{15}N-TROSY spectra were measured before and after DCCD incubation for 3 h.

Gaussian Network Model analysis. Normal modes were calculated for the mVDAC1 crystal structure (PDB code 3emn) using a standard C^α-atom based Gaussian Network Model available as online server oGNM (12). A default value of 10 Å was used as a cutoff (r_c) for construction of the Kirchhoff matrix using C^α-atoms.

MD simulation. MD simulations were performed using Gromacs 4.0 (13) together with the OPLS (14) and amber99sb force-fields (15), respectively, for the protein, water, and ions. The initial structure of mVDAC1 was taken from PDB structure 3EMN (16). Protonation states of the protein ionizable groups were determined using Whatif (17). mVDAC1 was embedded in an equilibrated and fully hydrated dimyristoylphosphatidylcholine (DMPC) bilayer derived from Berger et al. (18) comprising 392 lipid molecules by employing g_membed (19). The surrounding aqueous solution consisted of 13,953 water molecules using the TIP4P model (20) in the OPLS simulations, and of 12,937 water molecules employing the TIP3P model (20) in the case of amber99sb. The salt concentration was 0.15 M in all cases, using K^+ and Cl^- ions. In the OPLS simulations, eight K^+ and 11 Cl^- were used to neutralize the system. Hydrogen atoms were treated using the virtual sites approach in the OPLS simulations (21), allowing for an integration time-step of 4 fs. In the amber simulations, a time-step of 2 fs was used in connection with fully atomistic treatment of hydrogen atoms. The temperature was kept constant by weakly ($\tau = 0.1$ ps) coupling the lipids, protein, and solvent separately to a temperature bath of 320 K using the v-rescale method. The temperature was slightly raised to prevent transitions of DMPC into the gel phase. Likewise, the pressure in the system was kept constant by semiisotropic coupling to a pressure of 1 bar. Before the start of production runs, equilibration of the system was performed by applying position restraints of 1,000 kJ mol^{-1} nm^{-2} on the protein heavy atoms for 20 ns. Subsequently, trajectories totaling in a length of ~0.5 μs were obtained by free simulation.

To analyze slow and fast motions of mVDAC1, low- and high-pass filtering was applied on the trajectories. Calculated root mean square fluctuation (rmsF) values were transformed into isotropic B-factors and averaged using a running average of eight residues in length. A contribution of 1 Å to the total rmsF was assumed to arise from static disorder and subtracted.

Collective motions of mVDAC1 were analyzed by performing a principal component analysis (PCA) on the barrel backbone (amino acids 21-–283) and projecting the trajectories on the obtained eigenvectors. Elliptic fitting was carried out on eigenmode 1 using C_α positions. All molecular representations were generated using VMD (22). The lipid bilayer thickness was determined by measuring the average distance between the phosphate atoms of DMPC in the lower and upper leaflets using a grid-based approach based upon the GridMAT algorithm (23).

1. Engelhardt H, et al. (2007) High-level expression, refolding and probing the natural fold of the human voltage-dependent anion channel isoforms I and II. *J Membr Biol* 216:93–105.
2. Bayrhuber M, et al. (2008) Structure of the human voltage-dependent anion channel. *Proc Natl Acad Sci USA*105:15370–15375.
3. Hiller S, et al. (2008) Solution structure of the integral human membrane protein VDAC-1 in detergent micelles. *Science* 321:1206–1210.
4. Delaglio F, et al. (1995) NMRPipe: a multidimensional spectral processing system based on UNIX pipes. *J Biomol NMR* 6:277–293.
5. Goddard TD, Kneller DG (2006) *SPARKY 3* University of California San Francisco. http://www.cgl.ucsf.edu/home/sparky/
6. Eletsky A, Kienhofer A, Pervushin K (2001) TROSY NMR with partially deuterated proteins. *J Biomol NMR* 20:177–180.
7. Zhu G, Kong XM, Sze KH (1999) Gradient and sensitivity enhancement of 2D TROSY with water flip-back, 3D NOESY-TROSY and TOCSY-TROSY experiments. *Journal of Biomolecular NMR* 13:77–81.
8. Schneider R, et al. (2010) The native conformation of the human VDAC1 N terminus. *Angew Chem Int Ed Engl* 49:1882–1885.
9. Zhu G, Xia Y, Nicholson LK, Sze KH (2000) Protein dynamics measurements by TROSY-based NMR experiments. *J Magn Reson* 143:423–426.
10. Wang C, Rance M, Palmer AG III (2003) Mapping chemical exchange in proteins with MW > 50 kD. *J Am Chem Soc* 125:8968–8969.
11. Fushman D, et al. (1998) The solution structure and dynamics of the pleckstrin homology domain of G protein-coupled receptor kinase 2 (beta-adrenergic receptor kinase 1). A binding partner of Gbetagamma subunits. *J Biol Chem* 273:2835–2843.
12. Yang LW, et al. (2006) oGNM: online computation of structural dynamics using the Gaussian Network Model. *Nucleic Acids Res* 34:W24–31.
13. Hess B, Kutzner C, van der Spoel D, Lindahl E (2008) GROMACS 4: Algorithms for highly efficient, load-balanced, and scalable molecular simulation. *Journal of Chemical Theory and Computation* 4:435–447.
14. Jorgensen WL, Maxwell DS, Tirado-Rives J (1996) Development and testing of the OPLS all-atom force field on conformational energetics and properties of organic liquids. *Journal of the American Chemical Society* 118:11225–11236.
15. Wang J, Wolf RM, Caldwell JW, Kollman PA, Case DA (2004) Development and testing of a general amber force field. *J Comput Chem* 25:1157–1174.
16. Ujwal R, et al. (2008) The crystal structure of mouse VDAC1 at 2.3 A resolution reveals mechanistic insights into metabolite gating. *Proc Natl Acad Sci USA* 105:17742–17747.
17. Vriend G (1990) WHAT IF: a molecular modeling and drug design program. *J Mol Graph* 8:52–56, 29.
18. Berger O, Edholm O, Jahnig F (1997) Molecular dynamics simulations of a fluid bilayer of dipalmitoylphosphatidylcholine at full hydration, constant pressure, and constant temperature. *Biophys J* 72:2002–2013.
19. Wolf MG, Hoefling M, Aponte-Santamaria C, Grubmuller H, Groenhof G (2010) g_membed: Efficient insertion of a membrane protein into an equilibrated lipid bilayer with minimal perturbation. *J Comput Chem* 31:2169–2174.
20. Jorgensen WL, Chandrasekhar J, Madura JD, Impey RW, Klein ML (1983) Comparison of simple potential functions for simulating liquid water. *The Journal of Chemical Physics* 79:926–935.
21. Feenstra KA, Hess B, Berendsen HJC (1999) Improving efficiency of large time-scale molecular dynamics simulations of hydrogen-rich systems. *Journal of Computational Chemistry* 20:786–798.
22. Humphrey W, Dalke A, Schulten K (1996) VMD: visual molecular dynamics. *J Mol Graph* 14:33–38, 27–38.
23. Allen WJ, Lemkul JA, Bevan DR (2009) GridMAT-MD: a grid-based membrane analysis tool for use with molecular dynamics. *J Comput Chem* 30:1952–1958.
24. DeLano WL (2003) PyMOL Reference Manual. DeLano Scientific LLC, San Carlos, CA.

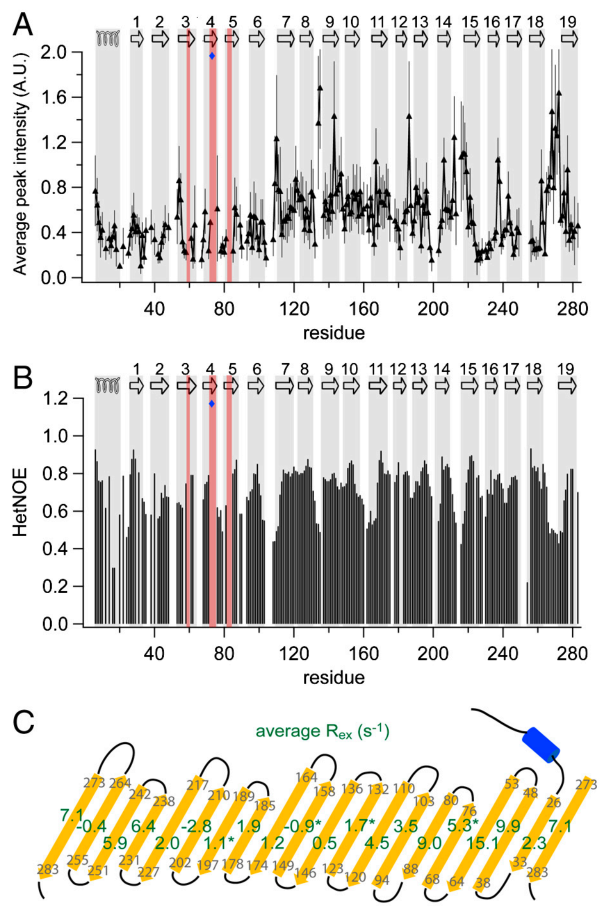

Fig. S1. *Details of hVDAC1 dynamics*. (*A*) Average peak intensities (mean ± s.d., $n = 3$) of WT VDAC1 from two-dimensional ^{1}H,^{15}N-TROSY spectra measured at 900 MHz. (*B*) Heteronuclear NOE values (HetNOE) of hVDAC1 measured at 800 MHz. Intensity ratios were averaged over a three-residue window. (*A*) and (*B*) The topology of hVDAC1 is indicated on top, with secondary structure elements highlighted in gray. Residues that could not be assigned are highlighted in red, E73 is indicated by a blue diamond. (*C*) Topology map of hVDAC1 showing average R_{ex} values for all β-strands in green. β-strands with first and last residue (gray) are indicated as yellow arrows, the N-terminal helix as a blue cylinder. Average R_{ex} value obtained after removal of negative outliers with values < −12 are marked with an asterisk.

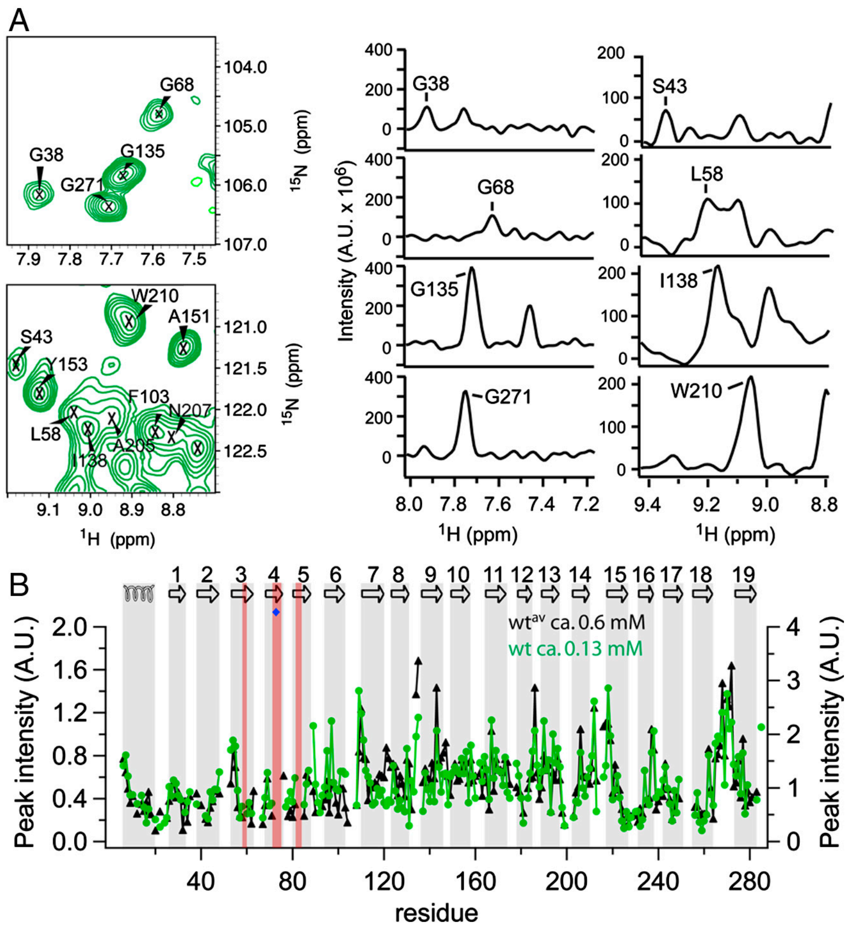

Fig. S2. *Effects of dilution onto peak intensities*. (*A*) Enlarged spectral regions and one-dimensional traces of a ^{1}H,^{15}N-TROSY spectrum of diluted hVDAC1 (0.13 mM) measured at a ^{1}H frequency of 900 MHz showing examples of broadened and nonbroadened peaks. (*B*) Absolute peak intensity for diluted (~0.13 mM; green circles) and the average peak intensities (mean, $n = 3$) of concentrated WT hVDAC1 (~0.6 mM; black triangles) from two-dimensional ^{1}H,^{15}N-TROSY spectra. The topology of VDAC1 is indicated on top, with secondary structure elements highlighted in gray. Residues that could not be assigned are highlighted in red; E73 is indicated by a blue diamond.

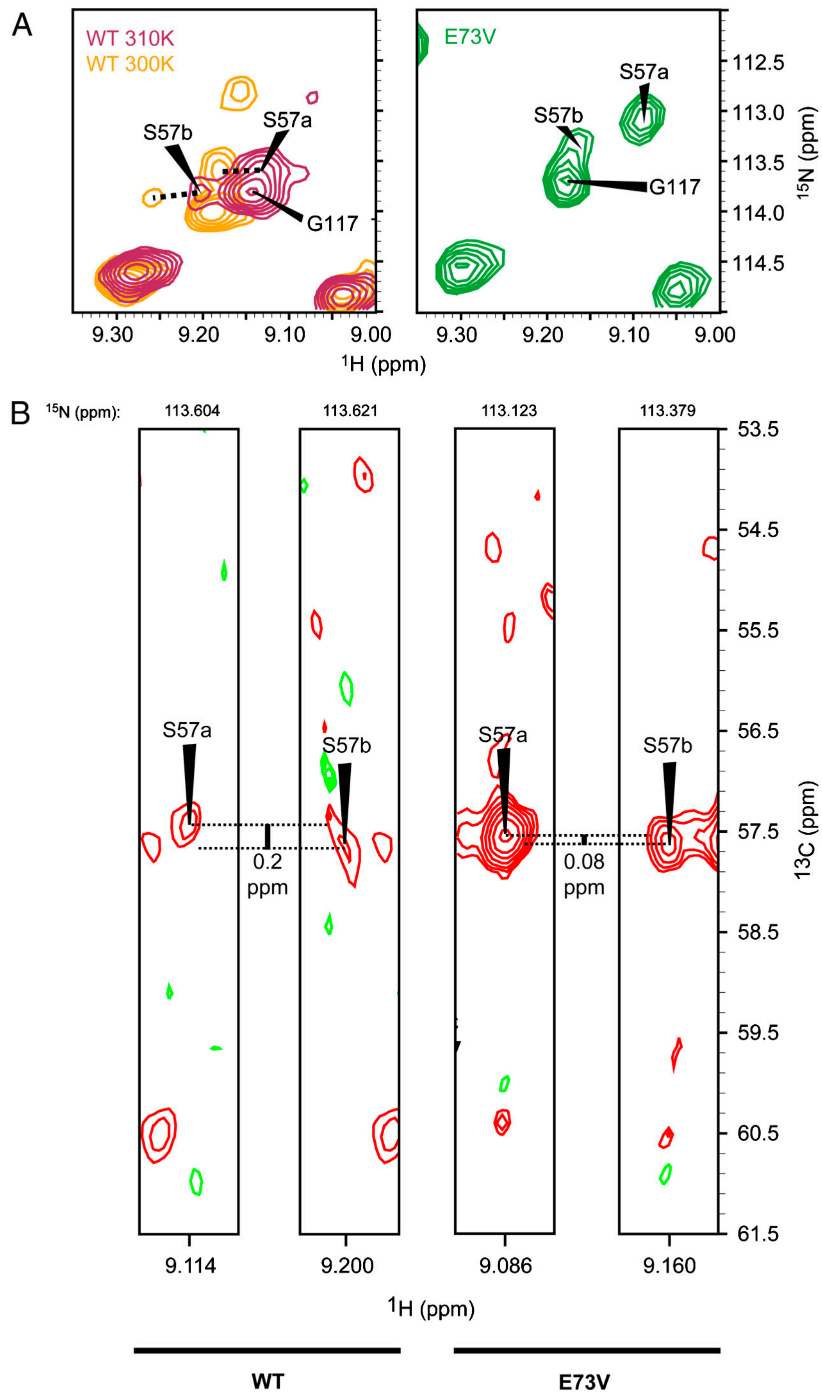

Fig. S3. *Chemical exchange of residue S57*. (*A*) Enlarged spectral regions of ^{1}H,^{15}N-TROSY spectra of WT and E73V hVDAC1 measured at 900 MHz showing the two resonances of S57 (S57a and S57b). The dashed lines indicate the temperature-dependent shift of both resonances. (*B*) Two-dimensional ^{1}H,^{13}C-strips from three-dimensional TROSY-HNCA spectra of WT and E73V hVDAC1 measured at 900 MHz showing the S57 resonances. The dashed lines indicate the differences in C_α chemical shift.

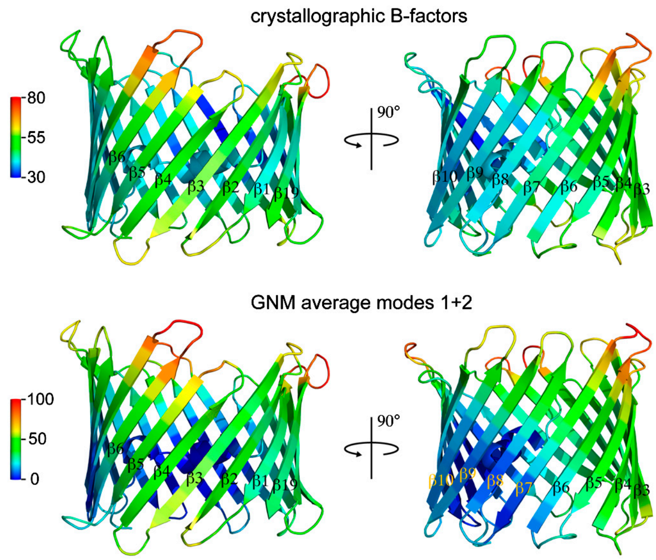

Fig. S4. *Structural mapping of crystallographic B-factors and GNM-predicted mobility.* Cartoon representations of mVDAC1 generated from the crystal structure (PDB code 3emn) using PyMOL (24), color-coded by crystallographic B-factors and GNM-predicted residue fluctuations for the average of the two lowest frequency modes, rescaled by the oGNM server (12) to yield effective B-factors.

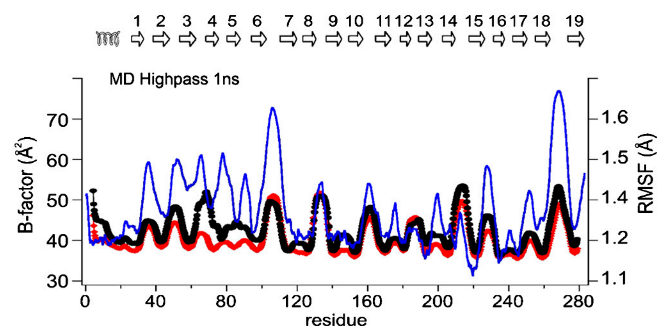

Fig. S5. Fast motions of the barrel of mVDAC1 as deduced from the MD simulation (red, E73⁻ and black, E73º), compared with the X-ray crystallographic B-factors (blue).

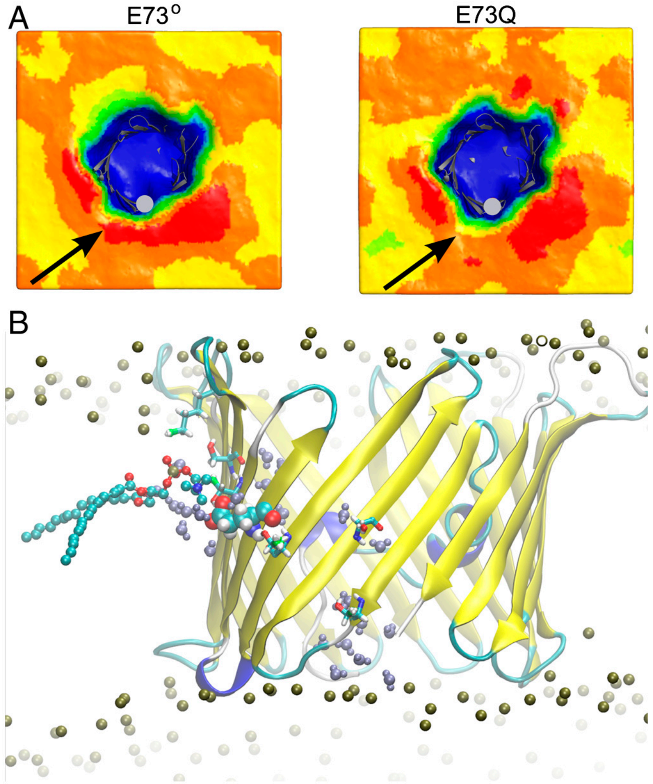

Fig. S6. (*A*) Membrane thickness around E73 in mVDAC1 for the case E73° and the mutant E73Q. Color code as in Fig. 3, main text. (*B*) DMPC lipid flipping induced by an interaction between the DMPC head group and E73 of mVDAC1.

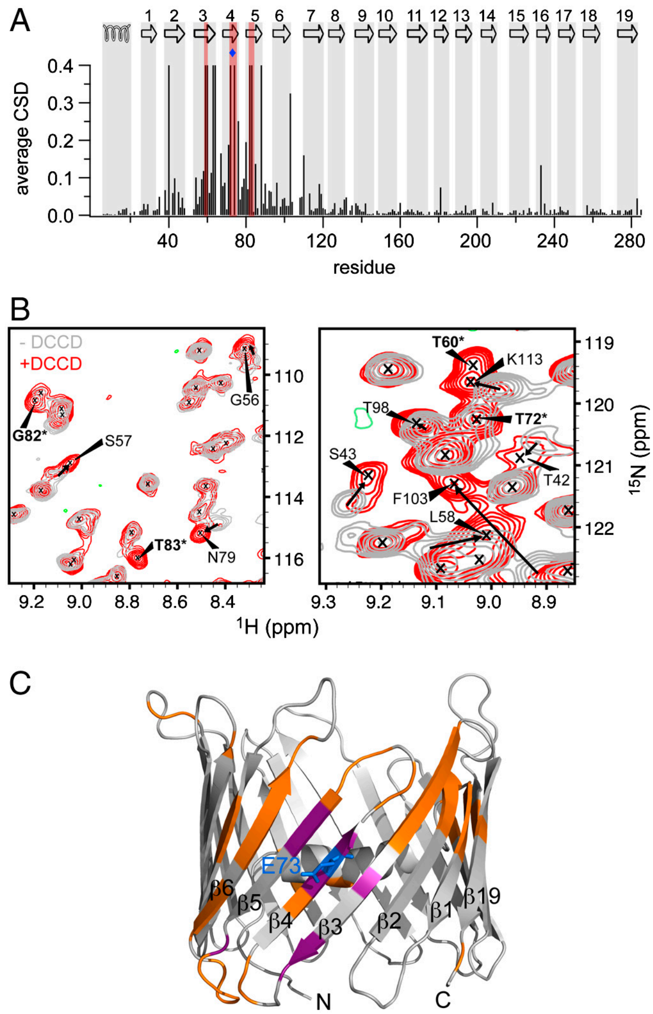

Fig. S7. *DCCD-induced changes in hVDAC1 dynamics.* (*A*) Average chemical shift distribution, CSD $= ((0.2\Delta\delta N)^2 + \Delta\delta H^2)/2)^{1/2}$, from ^{1}H,^{15}N-TROSY spectra. The topology of hVDAC1 is indicated on top, with secondary structure elements highlighted in gray. Residues that could not be assigned are highlighted in red, E73 is indicated by a blue diamond. (*B*) Enlarged spectral regions of a ^{1}H,^{15}N-TROSY spectrum before (gray) and after (red) incubation with DCCD. Shifting peaks are indicated by arrows, newly appearing or strongly increased peaks are printed in bold and labeled with an asterisk. (*C*) Cartoon representation of hVDAC1 with residues that show an average intensity ratio >1.2 (DCCD-bound compared to reference hVDAC1) mapped in orange. Residues that show up after DCCD treatment are colored in purple.